crystals

MDPI

*Article*

# Hafnium Carbide: Prediction of Crystalline Structures and Investigation of Mechanical Properties

**Jelena Zagorac [1,2,*], Johann Christian Schön [3,*], Branko Matović [1,2], Svetlana Butulija [1,2] and Dejan Zagorac [1,2]**

[1] Materials Science Laboratory, Institute of Nuclear Sciences Vinča, Belgrade University, 11000 Belgrade, Serbia; mato@vinca.rs (B.M.); svetlana8@vin.bg.ac.rs (S.B.); dzagorac@vinca.rs (D.Z.)
[2] Center for Synthesis, Processing and Characterization of Materials for Application in the Extreme Conditions-CextremeLab, Materials Science Laboratory, Institute of Nuclear Sciences Vinča, 11000 Belgrade, Serbia
[3] Max Planck Institute for Solid State Research, Heisenbergstr. 1, 70569 Stuttgart, Germany
* Correspondence: jelena@vinca.rs (J.Z.); c.schoen@fkf.mpg.de (J.C.S.)

**Abstract:** Hafnium carbide (HfC) is a refractory compound known for its exceptional mechanical, thermal, and electrical properties. This compound has gained significant attention in materials science and engineering due to its high melting point, extreme hardness, and excellent thermal stability. This study presents crystal structure prediction via energy landscape explorations of pristine hafnium carbide supplemented by data mining. Apart from the well-known equilibrium rock salt phase, we predict eight new polymorphs of HfC. The predicted HfC phases appear in the energy landscape with known structure types such as the WC type, NiAs type, 5-5 type, sphalerite (ZnS) type, TlI type, and CsCl type; in addition, we predict two new structure types denoted as *ortho*_HfC and HfC_*polytype*, respectively. Moreover, we have investigated the structural characteristics and mechanical properties of hafnium carbide at the DFT level of computation, which opens diverse applications in various technological domains.

**Keywords:** hafnium carbide; structure prediction; mechanical properties



**Citation:** Zagorac, J.; Schön, J.C.; Matović, B.; Butulija, S.; Zagorac, D. Hafnium Carbide: Prediction of Crystalline Structures and Investigation of Mechanical Properties. *Crystals* **2024**, *14*, 340. https://doi.org/10.3390/cryst14040340

Academic Editors: Nektarios N. Lathiotakis and Zacharias G. Fthenakis

Received: 9 March 2024
Revised: 19 March 2024
Accepted: 25 March 2024
Published: 2 April 2024



## 1. Introduction

The lack of predictability in solid-state synthesis and crystallography makes it difficult to discover new crystalline structures and design new materials. This is of particular concern since new types of crystal structures can exhibit special physical and chemical properties, while their realization as new materials is of great technological interest. To enhance crystal structure and materials discovery by providing promising synthesis targets in given chemical systems, the prediction of possible crystal structures in a chemical system and the computation of their physical properties are therefore of vital importance [1]. Here, crystal structure prediction (CSP) refers to the determination of the feasible crystalline modifications of solids from first principles, i.e., without input from experiments, where a large variety of search methods have been employed [1–9]; these a priori-type methods are frequently supplemented by data mining procedures that suggest starting configurations for local minimizations on the landscape. The ability to perform such predictions is based on the underlying mathematical structure of the chemical system, the energy landscape [10], where the time evolution and dynamics of the system occur, and where stable compounds correspond to locally ergodic regions on the landscape [2]. Thus, the study of the energy landscape of a chemical system provides insight into metastable chemical compounds capable of existence on various observational time scales [10] ranging from simple molecules and clusters [11], biomolecules [11], monolayers and nanotubes [12], bulk crystalline [7], and amorphous solids [11] to phase diagrams of multinary chemical systems [13] including both thermodynamically stable and metastable phases [14]. The energy landscape concepts and their applications in extreme conditions [15] are especially important for investigating

materials such as hafnium carbide, where not only the potential energy landscape but also the potential enthalpy landscapes [10] at high non-zero pressures are relevant.

Hafnium carbide (HfC) belongs to the family of transition metal carbides and exhibits a wide range of remarkable properties including high strength, wear resistance, anti-oxidation, anti-corrosion, and biocompatibility, which make it a promising candidate for advanced materials applications [16]. It also ranks among the hardest materials, with a Vickers hardness value exceeding 20 GPa, making it a possible substitute for industrial diamonds [17]. Its high melting point, approximately 3900 °C, has attracted interest since a superior level of hardness can be inferred from a high melting point [18]. HfC can form solid solutions with various chemical systems, e.g., with TaC [19], ZrC [20], SiC [21], uranium monocarbide (UC) [22], and more complex ones like (Hf, Ta)C/SiC, and (Hf, Ti)C/SiC [23], SiC/(Hf, Ta)C(N)/(B)C [24], etc.

Several methods have been developed for synthesizing hafnium carbide, including carbothermic reduction, low-temperature synthesis, sol–gel polycondensation, chemical vapor deposition (CVD), and spark plasma sintering (SPS) [25–28]. In all of these experiments, as well as most of the calculations reported in the literature, hafnium carbide adopts a face-centered cubic (FCC) crystal structure, similar to that of the rock salt (NaCl) type [17,29–31]. In most of the earlier theoretical work, the equilibrium NaCl structure has been investigated for its mechanical properties, especially regarding the Vickers hardness [32–36]. There is only one study, by Zeng et al. [35], that deals with other HfC phases; however, the stable hafnium carbides discussed exhibit stoichiometries different from HfC.

In the current study, we go beyond this earlier work in a systematic fashion by performing a priori structure prediction in pristine hafnium carbide. We identify novel HfC modifications and compute their mechanical properties, thus providing promising targets for the synthesis of new HfC-based materials.

## 2. Computational Details

In the first part of our study, crystal structure prediction of hafnium carbide was carried out using global optimization (GS) of the energy landscape for identifying local minima of the potential energy or enthalpy. This exploration was supplemented by results from data mining-based searches, followed by local optimizations on the ab initio level of the most promising candidate structures, similar to the general procedure used in earlier work [37].

The enthalpy landscape of the HfC compound was explored for several pressures, including extremely high values up to $1.6 \times 10^6$ GPa (0, 0.16, 1.6, 16, 160, 1600, 16,000, 160,000 and 1,600,000 GPa). Here, we employed simulated annealing as an algorithm for the global search, combined with periodic local optimizations along the search trajectory, carried out with the G42+ code [38]. The global searches were performed for four formula units of HfC, and the moveclass of the random walk included shifts in randomly selected atoms only (65%), exchange of randomly chosen pairs of atoms (10%), and changes in the cell parameters with and without atom movements (25%). To perform the global searches with a reasonable computational effort, a fast computable empirical two-body potential consisting of Lennard–Jones and exponentially damped Coulomb terms was employed. In this fashion, ca. 27,000 structure candidates exhibiting a great variety of structures and structure types were generated.

The global search was supplemented with data-mining-based explorations of the ICSD database [39,40], which were restricted to the common AB structure prototypes found in our previous studies [41,42]. The data mining confirmed the equilibrium rock salt (NaCl), cesium chloride (CsCl), and sphalerite (ZnS) types of structures that had been obtained from the global searches as feasible modifications, and added the tungsten carbide (WC) type as a structure candidate in the HfC system via analogy to known crystallographic structure types.

The final step of the structure prediction part of the study was accomplished by locally minimizing all promising structure candidates on an ab initio level with the CRYSTAL17

code, based on linear combinations of atomic orbitals [43,44]. Analytical gradients were used for the local optimization [45,46]. DFT calculations were performed using two different functionals and approximations: the local density approximation (LDA) with the Perdew–Zunger (PZ) correlation functional [47], and the generalized gradient approximation (GGA) with the Perdew–Burke–Ernzerhof (PBE) functional [48]. Previous studies have shown that the choice of these DFT functionals produces reliable structure prediction results [37,41]. For the integration over the Brillouin zone, a k-point mesh of $8 \times 8 \times 8$ was generated using the Monkhorst–Pack scheme [49], and the energy convergence tolerance was set as $10^{-7}$ eV/atom [50].

Basis set choice is very important for the correct DFT structure optimization [51]. For hafnium, a Hf_ECP_Stevens_411d31G_munoz_2007 effective core pseudopotential was employed [52]. In the case of carbon, the C_6-21G*_catti_1993 all-electron basis set based on Gaussian-type orbitals was used [53,54].

Subsequently, the symmetries of the computed structures were determined using the program KPLOT [55], and the structures were visualized using the Vesta code [56]. Next, the energy was computed as a function of volume for the most promising modifications predicted, and possible high-temperature and high-pressure or effective negative-pressure phases were identified.

Finally, in the second part of this study, the mechanical properties of selected particularly interesting crystalline HfC structure candidates were calculated using the computational strategy implemented in the CRYSTAL17 solid-state quantum-chemical program [57]. A full elastic tensor has been generated using the keyword ELASTCON [58].

## 3. Results and Discussion

### *3.1. Energy Landscape and Energetic Properties*

The most common candidate we observe on the enthalpy landscapes of HfC appears in the rock salt (NaCl) structure, which is the lowest energy minimum (global minimum) on the empirical potential energy landscape of HfC. After local optimization on the DFT level using LDA-PZ and GGA-PBE functionals, the NaCl type modification continues to be the lowest energy structure, shown on the computed energy vs. volume, E(V), curves (Figure 1) as well as in the energy ranking (Table 1). This is in agreement with the experimental observations [17] where it has been observed that NaCl is the equilibrium structure at standard thermodynamic conditions.

**Table 1.** Energy ranking of the crystalline structure candidates after ab initio optimization. The total energy (in Eh) is computed using the LDA-PZ and GGA-PBE functional.

| Modification | LDA | PBE |
|---|---|---|
| NaCl_type | −86.6624 | −87.0498 |
| *Ortho*_HfC_type | −86.6428 | −87.0319 |
| 5-5_type | −86.6352 | −87.0261 |
| HfC_*polytype* | −86.6324 | −87.0203 |
| TlI_type | −86.6251 | −87.0135 |
| NiAs_type | −86.6209 | −87.0104 |
| WC_type | −86.6055 | −86.9942 |
| ZnS_type | −86.6034 | −86.9968 |
| CsCl_type | −86.5664 | −86.9519 |

Apart from the NaCl modification, we note three predicted structures possibly appearing for effective negative pressures: the new *ortho*_HfC type, the 5-5 type, and the ZnS type (Figure 1 and Table 1). Similarly, several new polymorphs for the HfC system are predicted that might be feasible at high pressures or in the high-temperature region of the phase diagram, exhibiting the TlI type, the NiAs type, the WC type, and a new HfC_*polytype*. The CsCl type only appears on the enthalpy landscape for extremely high pressures and is energetically quite high compared to the other predicted modifications

(Figure 1 and Table 1), suggesting that it might be difficult to reach even in high-pressure experiments, in contrast to, e.g., the case of most alkali metal halides [42]. We note that the energy ranking of these HfC polymorphs remains the same regardless of the computational ab initio approach employed, with only a slight variation between the WC and the ZnS type at the GGA-PBE level (Table 1).

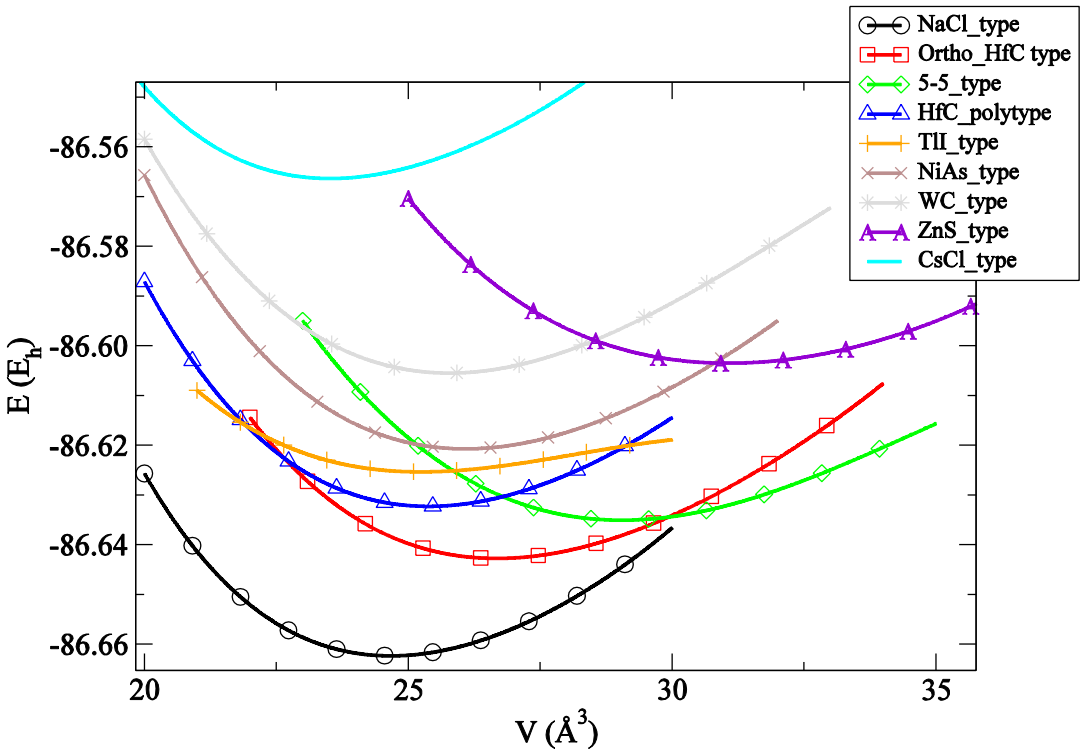


**Figure 1.** Energy vs. volume, E(V), curves for the nine most stable and energetically favorable structure candidates in the HfC system obtained using the LDA functional. Energies per formula unit are given in Hartree (Eh).

### *3.2. Crystal Structure Prediction and Polymorphs of HfC*

The predicted structures of hafnium carbide are visualized in Figure 2, while full structural details computed using LDA and GGA are presented in Table 2. The global minimum is found in the rock salt (NaCl) type of structure (Figure 2a) and appears in the cubic symmetry with the space group *Fm*-3*m* (no. 225), which is the known equilibrium phase of hafnium carbide. We note that the computed unit cell parameters (LDA $a$ = 4.62 Å, GGA $a$ = 4.67 Å, Table 2) are in excellent agreement with previous experimental observations [16,59–62] and DFT calculations [34,63–69].

The so-called 5-5 type is predicted to be thermodynamically stable in the negative pressure region (Figure 1). The transition negative pressure is expected to be around −20 GPa. The 5-5 structure type appears in the hexagonal symmetry with space group $P6_3/mmc$ (no. 194). This type of structure can be described as a mutual fivefold coordination of cation A by anion B in a hexagonal lattice with *ABAB* stacking, where the A-atoms form trigonal bipyramids around B-atoms, and vice versa (Figure 2b) [70]. This structure has been found on the energy landscape of various *AB* chemical systems in the past [42,70–72].

The new predicted *ortho*_HfC type of structure appears in orthorhombic symmetry with space group *Cmcm* (no. 63) (Table 2). This new structure type can be visualized as a combination of the NaCl and 5-5 types of structure, where six fold octahedra are edge connected to the five fold trigonal bipyramids (Figure 2c), reminiscent of an intergrowth type of structure. Such a combination of structural features has reduced symmetry to the orthorhombic lattice; however, it should be feasible to synthesize it on the NaCl →

5-5 transition route. This is supported by the observation that very similar kinds of combinations of octahedra and trigonal bipyramids have been observed as local minima on the energy landscape of other ionic systems, such as for bulk NaCl (c.f., Figure 3 in reference [70]) or monolayers of MgO on sapphire (c.f., Figure 3d in reference [38]). Another novel structure type has also been found as a polytypic form of hafnium carbide, which is the first report of its kind. The HfC_*polytype* modification appears in the *R*3*m* (no. 160) space group in the trigonal crystal system (Figure 2d). The polytypic structure consists of edge-connected six-fold octahedra and trigonal prisms, which we might consider as a combination of NiAs and WC structural features. The trigonal symmetry of the HfC_*polytype* remains high and can easily be transformed into a hexagonal setting (shown in Table 2 and Figure 2d). The polytypic behavior has previously been experimentally observed in various chemical systems [73–75] and theoretically computed [76,77] in various chemical systems; in the HfC compound, it appears in high-temperature conditions as a metastable phase (Figure 1).

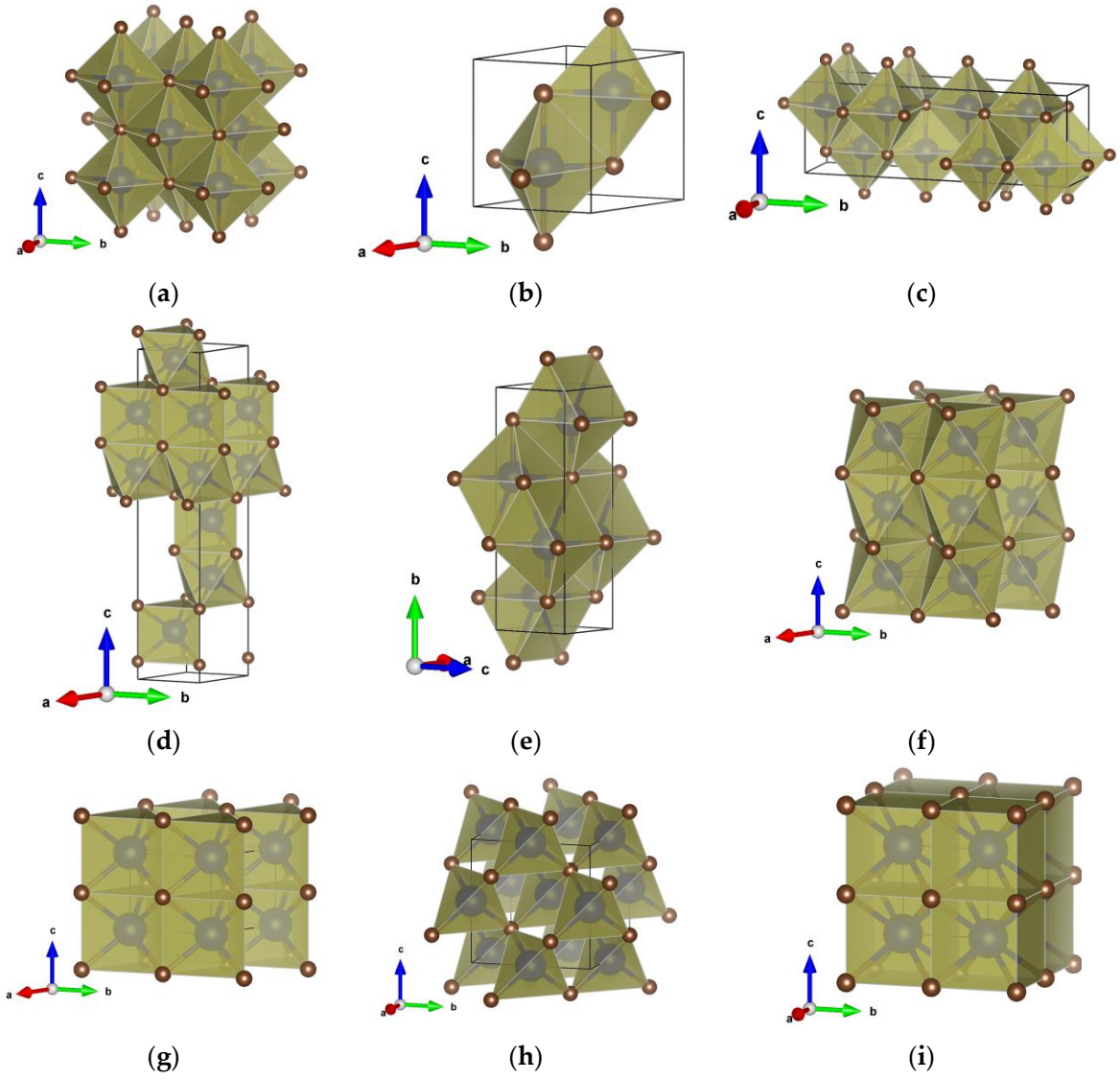


**Figure 2.** Predicted HfC structure candidates from global search: (**a**) NaCl_type; (**b**) 5-5_type: (**c**) *Ortho*_HfC_type; (**d**) HfC_*polytype*; (**e**) TlI_type; (**f**) NiAs_type; (**g**) WC_type; (**h**) ZnS_type; (**i**) CsCl_type. Hf ions are shown as large blue spheres inside the coordination polyhedra, and C ions are shown as small golden spheres at the corners of the coordination polyhedra.

**Table 2.** Structure type, space group, unit cell parameters (Å), unit cell volume (Å$^3$), and atomic positions for the most relevant HfC polymorphs.

| Structure Candidates | LDA | PBE |
|---|---|---|
| NaCl_type | *Fm*-3*m* (225)<br>*a* = 4.62; *V* = 98.51<br>Hf 0 0 0<br>C 1/2 0 0 | *Fm*-3*m* (225)<br>*a* = 4.67; *V* = 101.91<br>Hf 0 0 0<br>C 1/2 0 0 |
| Ortho_HfC type | *Cmcm* (63)<br>*a* = 3.40; *b* = 13.66; *c* = 4.59; *V* = 213.30<br>Hf1 0 0.6862 1/4<br>Hf2 0 0.9200 1/4<br>C1 0 0.3144 1/4<br>C2 0 0.0799 1/4 | *Cmcm* (63)<br>*a* = 3.45; *b* = 13.81<br>*c* = 4.64; *V* = 220.66<br>Hf1 0 0.6857 1/4<br>Hf2 0 0.9201 1/4<br>C1 0 0.3149 1/4<br>C2 0 0.0799 1/4 |
| 5-5_type | $P6_3/mmc$ (194)<br>*a* = 3.82; *c* = 4.60; *V* = 58.01<br>Hf 1/3 2/3 3/4<br>C 2/3 1/3 3/4 | $P6_3/mmc$ (194)<br>*a* = 3.86; *c* = 4.65<br>*V* = 60.02<br>Hf 1/3 2/3 3/4<br>C 2/3 1/3 3/4 |
| HfC_*polytype* | *R*3*m* (160)<br>*a* = 3.24; *c* = 16.73; *V* = 152.34<br>Hf1 0 0 0.8085<br>Hf2 0 0 0.6344<br>C1 0 0 0.2234<br>C2 0 0 0.0541 | *R*3*m* (160)<br>*a* = 3.28; *c* = 16.90<br>*V* = 157.70<br>Hf1 0 0 0.8085<br>Hf2 0 0 0.6345<br>C1 0 0 0.2234<br>C2 0 0 0.0540 |
| TlI_type | *Cmcm* (63)<br>*a* = 3.15; *b* = 9.54; *c* = 3.34; *V* = 100.52<br>Hf 0 0.6343 1/4<br>C 0 0.8697 1/4 | *Cmcm* (63)<br>*a* = 3.20; *b* = 9.92<br>*c* = 3.35; *V* = 106.16<br>Hf 0 0.6367 1/4<br>C 0 0.8649 1/4 |
| NiAs_type | $P6_3/mmc$ (194)<br>*a* = 3.24; *c* = 5.72; *V* = 52.03<br>Hf 0 0 1/2<br>C 1/3 2/3 3/4 | $P6_3/mmc$ (194)<br>*a* = 3.28; *c* = 5.78<br>*V* = 53.86<br>Hf 0 0 0.5<br>C 1/3 2/3 3/4 |
| WC_type | *P*-6*m*2 (187)<br>*a* = 3.20; *c* = 2.90; *V* = 25.73<br>Hf 0 0 0<br>C 1/3 2/3 1/2 | *P*-6*m*2 (187)<br>*a* = 3.24; *c* = 2.93<br>*V* = 26.68<br>Hf 0 0 0<br>C 1/3 2/3 1/2 |
| ZnS_type | *F*-43*m* (216)<br>*a* = 4.99; *V* = 124.33<br>Hf 1/2 1/2 1/2<br>C 3/4 3/4 1/4 | *F*-43*m* (216)<br>*a* = 5.05; *V* = 128.72<br>Hf 1/2 1/2 1/2<br>C 3/4 3/4 1/4 |
| CsCl_type | *Pm*-3*m* (221)<br>*a* = 2.87; *V* = 23.54<br>Hf 0 0 0<br>C 1/2 1/2 1/2 | *Pm*-3*m* (221)<br>*a* = 2.91; *V* = 24.54<br>Hf 0 0 0<br>C 1/2 1/2 1/2 |

The TlI structure type is predicted to appear as a high-temperature form of hafnium carbide (Figure 1, Table 1). Although the TlI modification exhibits the same orthorhombic space group *Cmcm* (no. 63) as the newly predicted *ortho*_HfC type, these two structures are different. Unit cell and structural parameters differ (Table 2) and the TlI structure shows a sevenfold coordination of Hf by C atoms. The orthorhombic TlI type can be considered to be a rather distorted NaCl structure type, described as a chain of monocapped trigonal

prisms sharing common rectangular faces (Figure 2e). There are possible synthesis routes for the TlI type of structure since it has previously been found along the NaCl → CsCl transition route in other chemical systems [41,78–80].

NiA modification appears in the same hexagonal $P6_3/mmc$ (no. 194) space group as the 5-5 type structure; however, they are structurally very different. The NiAs type shows sixfold coordination of hafnium by carbon forming *ABAB* layers of octahedra, while the 5-5 type is fivefold coordinated with trigonal bipyramids (Figure 2b,f), reminiscent of an ionic analog of the h-BN type structure. The NiAs type has been found in previous theoretical searches for various AB systems [42,70,71,78], but this is the first indication of this type in the hafnium carbide system.

The tungsten carbide (WC) type of structure shows a hexagonal lattice with space group *P*-6*m*2 (no. 187) (Table 2). The WC modification can be visualized as edge-connected trigonal prisms formed by the six-fold coordination of Hf atoms by C atoms (Figure 2g). The WC type of hafnium carbide has previously been theoretically investigated for its hardness and elastic properties [81], as well as for semi-metal and electronic properties [82]. We note that the calculated cell parameters for the WC structure (LDA $a$ = 3.20 Å; $c$ = 2.90 Å, GGA $a$ = 3.24 Å; $c$ = 2.93 Å) are in good agreement with previous DFT calculations (LDA $a$ = 3.227 Å; $c$ = 2.915Å, GGA $a$ = 3.267 Å; $c$ = 2.942 Å) [81,82].

Finally, we predict two cubic phases, exhibiting the ZnS and CsCl type, respectively, as structure candidates in the HfC system. Both commonly appear on the energy landscape of AB compounds [70]; however, they are structurally very different. The sphalerite (ZnS) type appears in the space group *F*-43*m* (no. 216) and the CsCl type in the space group *Pm*-3*m* (no. 221), respectively. The ZnS-like phase shows fourfold coordination of Hf ions by C ions, while in the CsCl-like one, the Hf ion is eightfold coordinated by C ions (Figure 2h,i). Yang et al. carried out first-principles calculations of mechanical properties of cubic 5d transition metal monocarbides, where they predicted a stable ZnS type and an unstable CsCl type modification of hafnium carbide [33]. Our DFT calculations of the unit cell parameters (Table 2) concur with this study [33].

### *3.3. Mechanical Properties of Hafnium Carbide*

The mechanical properties of hafnium carbide have been computed on the DFT-LDA level including elastic tensor constants ($C_{xy}$), bulk modulus (K), shear modulus (G), Young modulus (E), Poisson ratio (v), and Vickers hardness ($V_H$) as shown in Tables A1 and 3. The bulk modulus, shear modulus, and Vickers hardness were calculated using the Voigt–Reuss–Hill (VRH) approximation expressed in GPa. The Voigt–Reuss–Hill (VRH) approximation is a useful scheme by which anisotropic single-crystal elastic constants can be converted into isotropic polycrystalline elastic moduli, and where the validity of the VRH approximation is established in the literature [58,83]. Table 3 shows only three of the mechanically stable modifications of HfC, the NaCl type, the *ortho*_HfC type, and the NiAs type, and a comparison with previous experimental and theoretical observations where available. In addition, we will describe the computed mechanical properties of the mechanically unstable structures and compare them with previous reports in the literature. Here, instability was indicated by negative values of some of the computed elastic constants or/and mechanical moduli; we note that even though all structures investigated here corresponded to local minima of the energy and exhibited a positive bulk modulus (see Table A1 in Appendix A), such an instability can appear in the calculations due to the choice of approximation for the computation of the moduli and the finite atom displacements involved in the numerical computation of the moduli when the structure is already close to a possible phase transformation.

**Table 3.** Mechanical properties of hafnium carbide computed using LDA-PZ functional. Bulk modulus (K), shear modulus (G), and Vickers hardness ($V_H$) were calculated using the Voigt–Reuss–Hill (VRH) approximations expressed in GPa. We employed three different approximations for calculating the bulk and shear moduli and the Vickers hardness, where letters V, R, or H in the subscript denote the Voigt, Reuss, or Hill approach, respectively.

| Mechanical Property | Rock Salt (NaCl) Type | | | *ortho*_HfC Type | NiAs Type |
|---|---|---|---|---|---|
| | LDA | Experiment | Theory | LDA | LDA |
| Bulk modulus $K_V$ (GPa) | 261.54 | 242 [84], 263 [85] | 233 [63], 238 [86], 247 [33], 248 [87], 262.5 [68], 270 [36], 276.3 [34], 278 [35] | 228.12 | 230.53 |
| Bulk modulus $K_R$ (GPa) | 261.54 | | | 222.84 | 228.01 |
| Bulk modulus $K_H$ (GPa) | 261.54 | | | 225.48 | 229.27 |
| Shear modulus $G_V$ (GPa) | 195.08 | 195 [84] | 166 [32], 181 [33], 188.8 [34], 207 [35], 230 [36] | 86.10 | 146.79 |
| Shear modulus $G_R$ (GPa) | 192.38 | | | 237.31 | 132.56 |
| Shear modulus $G_H$ (GPa) | 193.73 | | | 161.71 | 139.67 |
| Young modulus $E_{-H}$ (GPa) | 466.11 | 430 [88], 461 [84] | 404 [32], 437 [33], 461.3 [34], 537 [36] | 391.53 | 348.29 |
| Poisson ratio $v_{-H}$ | 0.20 | n.a. | n.a. | 0.21 | 0.25 |
| Vickers (GPa) hardness $V_{H-V}$ | 27.57 | 26.1 [89], 18–20 [88] | 26.2 [33]; 29.08 [35] | 1.15 | 18.83 |
| Vickers (GPa) hardness $V_{H-R}$ | 26.87 | | | 47.48 | 15.80 |
| Vickers (GPa) hardness $V_{H-H}$ | 27.22 | | | 23.09 | 17.29 |

The computed value of the bulk modulus for the rock salt phase of HfC (K = 261.54 GPa) is in agreement with previous experimental (K = 242–263 GPa) and theoretical findings (233–278 GPa) (Table 3). Similarly, the computed values of the shear modulus (G = 192.73 GPa) and the Young modulus (E = 466.11 GPa) concur with experimental findings (G = 195 GPa and E = 461 GPa); here, the earlier calculations in the literature show a wide range of values (G = 166–230 GPa and E = 404–537 GPa). The computed Vickers hardness ($V_H$ = 27.22 GPa) is slightly overestimated compared to the data from experiment ($V_H$ = 18–26.1 GPa) but concurs with previously reported theoretical reports ($V_H$ = 26.2–29.08 GPa).

The computed bulk modulus (K = 225.48 GPa and 229.27 GPa), shear modulus (G = 161.71 GPa and 139.67 GPa), and Young modulus (E = 391.53 GPa and 348.29 GPa) for the predicted *ortho*_HfC-type and NiAs-type-HfC modifications are significantly lower than the values measured and computed for the equilibrium rock salt phase (Table 3). On the other hand, the computed Poisson ratio for these two predicted phases (v = 0.21 and 0.25) is higher than the one computed for the NaCl type modification. Finally, if one were to manage to synthesize the *ortho*_HfC type and the NiAs type of hafnium carbide, these would correspond to less hard phases compared to the rock salt type modification, and they thus might have versatile technological applications.

For the mechanically unstable structures (see Table A1 in Appendix A), we computed the value of the bulk modulus and compared it to previous calculations for the WC type, ZnS type, and CsCl type in the literature. Our LDA calculations of the bulk modulus of the WC type modification (K = 222.69 GPa) slightly underestimate the calculated values reported in the literature (K = 239 [81]), while for the ZnS type (K = 175.95 GPa) and the CsCl type (K = 227.16 GPa), we obtained slightly larger values (K = 165 GPa and K = 214 GPa [33]). We can conclude that our LDA-PZ calculations of the mechanical properties are in agreement with previous experimental and theoretical data, where available, and the values of the predicted mechanical properties of the new feasible HfC modifications should thus be realistic.

## 4. Conclusions

Hafnium carbide is a known compound with exceptional mechanical, thermal, and electrical properties. Here, we have performed crystal structure prediction of HfC using global optimization on enthalpy landscapes of the system supplemented by data mining searches in the ICSD database. Local optimizations of the obtained structure candidates have been performed using DFT, specifically employing the LDA-PZ and GGA-PBE functionals. Apart from the NaCl-type phase corresponding to the thermodynamically stable phase in standard conditions, we predict eight new polymorphs of hafnium carbide: the WC-type, NiAs-type, 5-5-type, ZnS-type, TlI-type, CsCl-type, *ortho*_HfC-type, and HfC_*polytype* polymorphs. Moreover, we have investigated the structural characteristics and mechanical properties of these predicted modifications of hafnium carbide at the ab initio level of computation. Our LDA-PZ calculations of the mechanical properties are in agreement with previous experimental and theoretical data, where available. The predicted values for the previously unknown HfC polymorphs suggest a certain degree of versatility for technological applications, making such modifications promising targets of chemical syntheses.

**Author Contributions:** D.Z., B.M. and J.C.S. conceived the idea; the global search optimization was performed by J.C.S., and the ab initio structure optimizations and the computation of the mechanical properties were performed by J.Z. and D.Z.; S.B. collected and analyzed the literature and the computational data. All authors contributed to the discussion and writing of the paper. All authors have read and agreed to the published version of the manuscript.

**Funding:** This research was funded by the Ministry of Science, Technological Development and Innovation of the Republic of Serbia through Contract No. 451-03-47/2023-01/200017.

**Data Availability Statement:** Data are contained within the article.

**Acknowledgments:** The authors are grateful to R. Dovesi, K. Doll, and Crystal Solutions for software support with CRYSTAL code.

**Conflicts of Interest:** The authors declare no conflicts of interest.

## Appendix A

**Table A1.** Bulk modulus (K) for the nine most promising predicted HfC structure types, calculated using the Voigt–Reuss–Hill (VRH) approximation, expressed in GPa.

| | NaCl_Type | *Ortho*_HfC _Type | 5-5_Type | HfC_*polytype* | TlI_Type | NiAs_Type | WC_Type | ZnS_Type | CsCl_Type |
|---|---|---|---|---|---|---|---|---|---|
| Bulk modulus $K_V$ | 261.54 | 228.12 | 208.70 | 237.89 | 209.70 | 230.53 | 224.23 | 179.95 | 227.16 |
| Bulk modulus $K_R$ | 261.54 | 222.84 | 205.11 | 237.86 | 131.91 | 228.01 | 221.16 | 175.95 | 227.16 |
| Bulk modulus $K_H$ | 261.54 | 225.48 | 206.90 | 237.87 | 170.80 | 229.27 | 222.69 | 175.95 | 227.16 |
| Exp | 242 [84]<br>263 [85] | n.a. | n.a. | n.a. | n.a. | n.a. | n.a. | n.a. | n.a. |
| Theory | 233 [63]<br>238 [86]<br>247 [33]<br>248 [87]<br>262.5 [68]<br>270 [36]<br>276.3 [34]<br>278 [35] | n.a. | n.a. | n.a. | n.a. | n.a. | 239 [81] | 165 [33] | 214 [33] |
| **Elastic tensor constants (GPa)** | $C_{11}$ = 560<br>$C_{12}$ = 112<br>$C_{44}$ = 175 | $C_{11}$ = 363<br>$C_{22}$ = 458<br>$C_{33}$ = 580<br>$C_{44}$ = 163<br>$C_{55}$ = 141<br>$C_{66}$ = 232<br>$C_{12}$ = 147<br>$C_{13}$ = 77<br>$C_{23}$ = 103 | $C_{11}$ = 253<br>$C_{12}$ = 241<br>$C_{13}$ = 86<br>$C_{33}$ = 550<br>$C_{44}$ = 142 | $C_{11}$ = 438<br>$C_{12}$ = 134<br>$C_{13}$ = 124<br>$C_{33}$ = 444<br>$C_{44}$ = −31 | $C_{11}$ = 525<br>$C_{22}$ = 166<br>$C_{33}$ = 520<br>$C_{44}$ = 165<br>$C_{55}$ = 235<br>$C_{66}$ = −833<br>$C_{12}$ = 18<br>$C_{13}$ = 164<br>$C_{23}$ = 152 | $C_{11}$ = 417<br>$C_{12}$ = 155<br>$C_{13}$ = 74<br>$C_{33}$ = 630<br>$C_{44}$ = 108 | $C_{11}$ = 420<br>$C_{12}$ = 146<br>$C_{13}$ = 57<br>$C_{33}$ = 661<br>$C_{44}$ = −70.29 | $C_{11}$ = 187<br>$C_{12}$ = 170<br>$C_{44}$ = 54 | $C_{11}$ = 83<br>$C_{12}$ = 299<br>$C_{44}$ = −252 |

## References


1. Schön, J.C.; Jansen, M. First Step Towards Planning of Syntheses in Solid-State Chemistry: Determination of Promising Structure Candidates by Global Optimization. *Angew. Chem. Int. Ed. Engl.* **1996**, *35*, 1286–1304. [CrossRef]
2. Schön, J.C.; Jansen, M. Determination, prediction, and understanding of structures, using the energy landscapes of chemical systems—Part I. *Z. Für Krist.-Cryst. Mater.* **2001**, *216*, 307–325. [CrossRef]
3. Wang, Y.; Lv, J.; Zhu, L.; Ma, Y. Crystal structure prediction via particle-swarm optimization. *Phys. Rev. B* **2010**, *82*, 094116. [CrossRef]
4. Wales, D.J. Energy Landscapes and Structure Prediction Using Basin-Hopping. In *Modern Methods of Crystal Structure Prediction*; Oganov, A.R., Ed.; John Wiley & Sons: Hoboken, NJ, USA, 2010; pp. 29–54.
5. Lyakhov, A.O.; Oganov, A.R.; Valle, M. Crystal Structure Prediction Using Evolutionary Approach. In *Modern Methods of Crystal Structure Prediction*; Oganov, A.R., Ed.; John Wiley & Sons: Hoboken, NJ, USA, 2010; pp. 147–180.
6. Woodley, S.M.; Catlow, R. Crystal structure prediction from first principles. *Nat. Mater.* **2008**, *7*, 937–946. [CrossRef] [PubMed]
7. Zurek, E. Discovering New Materials via A Priori Crystal Structure Prediction. *Rev. Comput. Chem.* **2016**, *29*, 274–326.
8. Oganov, A.; Pickard, C.; Zhu, Q.; Needs, R. Structure prediction drives materials discovery. *Nat. Rev. Mater.* **2019**, *4*, 331–348. [CrossRef]
9. Woodley, S.M.; Day, G.M.; Catlow, R. Structure prediction of crystals, surfaces and nanoparticles, Philosophical Transactions of the Royal Society A: Mathematical. *Phys. Eng. Sci.* **2020**, *378*, 20190600.
10. Schön, J.C. 3.11—Energy landscapes in inorganic chemistry. In *Comprehensive Inorganic Chemistry III*, 3rd ed.; Reedijk, J., Poeppelmeier, K.R., Eds.; Elsevier: Oxford, UK, 2023; Volume 3, pp. 262–392.
11. Wales, D. (Ed.) Introduction. In *Energy Landscapes: Applications to Clusters, Biomolecules and Glasses*; Cambridge University Press: Cambridge, UK, 2004; pp. 1–118.
12. Schön, J.C. Structure prediction in low dimensions: Concepts, issues and examples. *Philos. Trans. Ser. A Math. Phys. Eng. Sci.* **2023**, *381*, 20220246. [CrossRef] [PubMed]
13. Schön, J.C.; Jansen, M. Prediction, determination and validation of phase diagrams via the global study of energy landscapes. *Int. J. Mater. Res.* **2009**, *100*, 135–152. [CrossRef]
14. Jansen, M.; Pentin, I.V.; Schön, J.C. A Universal Representation of the States of Chemical Matter Including Metastable Configurations in Phase Diagrams. *Angew. Chem. Int. Ed.* **2012**, *51*, 132–135. [CrossRef]
15. Schön, J.C. Energy Landscape Concepts for Chemical Systems under Extreme Conditions. *J. Innov. Mater. Extrem. Cond.* **2021**, *2*, 5–57.
16. Nakamura, K.; Yashima, M. Crystal structure of NaCl-type transition metal monocarbides MC (M=V, Ti, Nb, Ta, Hf, Zr), a neutron powder diffraction study. *Mater. Sci. Eng. B* **2008**, *148*, 69–72. [CrossRef]
17. Cotter, P.G.; Kohn, J.A. Industrial Diamond Substitutes: I, Physical and X-Ray Study of Hafnium Carbide. *J. Am. Ceram. Soc.* **1954**, *37*, 415–420. [CrossRef]
18. Cedillos-Barraza, O.; Manara, D.; Boboridis, K.; Watkins, T.; Grasso, S.; Jayaseelan, D.D.; Konings, R.J.M.; Reece, M.J.; Lee, W.E. Investigating the highest melting temperature materials: A laser melting study of the TaC-HfC system. *Sci. Rep.* **2016**, *6*, 37962. [CrossRef]
19. Cedillos-Barraza, O.; Grasso, S.; Nasiri, N.A.; Jayaseelan, D.D.; Reece, M.J.; Lee, W.E. Sintering behaviour, solid solution formation and characterisation of TaC, HfC and TaC–HfC fabricated by spark plasma sintering. *J. Eur. Ceram. Soc.* **2016**, *36*, 1539–1548. [CrossRef]
20. Ghaffari, S.A.; Faghihi-Sani, M.A.; Golestani-Fard, F.; Nojabayy, M. Diffusion and solid solution formation between the binary carbides of TaC, HfC and ZrC. *Int. J. Refract. Met. Hard Mater.* **2013**, *41*, 180–184. [CrossRef]
21. Wen, Q.; Yu, Z.; Riedel, R.; Ionescu, E. Significant improvement of high-temperature oxidation resistance of HfC/SiC ceramic nanocomposites with the incorporation of a small amount of boron. *J. Eur. Ceram. Soc.* **2020**, *40*, 3499–3508. [CrossRef]
22. Krikorian, N.H.; Witteman, W.G.; Bowman, M.G. The Mutual Solid Solubility of Hafnium Carbide and Uranium Monocarbide. *J. Electrochem. Soc.* **1963**, *110*, 560. [CrossRef]
23. Wen, Q.; Riedel, R.; Ionescu, E. Significant improvement of the short-term high-temperature oxidation resistance of dense monolithic HfC/SiC ceramic nanocomposites upon incorporation of Ta. *Corros. Sci.* **2018**, *145*, 191–198. [CrossRef]
24. Bernauer, J.; Petry, N.-C.; Thor, N.; Kredel, S.A.; Teppala, D.T.; Galetz, M.; Lepple, M.; Pundt, A.; Ionescu, E.; Riedel, R. Exceptional Hardness and Thermal Properties of SiC/(Hf,Ta)C(N)/(B)C Ceramic Composites Derived from Single-Source Precursor. *Adv. Eng. Mater.* **2024**, 2301864. [CrossRef]
25. Yudin, S.N.; Kasimtsev, A.V.; Volodko, S.S.; Alimov, I.A.; Markova, G.V.; Sviridova, T.A.; Tabachkova, N.Y.; Buinevich, V.S.; Nepapushev, A.A.; Moskovskikh, D.O. Low-temperature synthesis of ultra-high-temperature HfC and HfCN nanoparticles. *Materialia* **2022**, *22*, 101415. [CrossRef]
26. Sacks, M.D.; Wang, C.-A.; Yang, Z.; Jain, A. Carbothermal reduction synthesis of nanocrystalline zirconium carbide and hafnium carbide powders using solution-derived precursors. *J. Mater. Sci.* **2004**, *39*, 6057–6066. [CrossRef]
27. Ha, D.; Kim, J.; Han, J.; Kang, S. Synthesis and properties of (Hf1-xTax)C solid solution carbides. *Ceram. Int.* **2018**, *44*, 19247–19253. [CrossRef]
28. Teppala, D.T.; Kredel, S.A.; Ionescu, E.; Matović, B. A Review of the Synthesis of Compositionally Complex Ultra-High-Temperature Ceramics. *J. Innov. Mater. Extrem. Cond.* **2023**, *4*, 77–103.

29. Elliott, R.O.; Kempter, C.P. Thermal Expansion of Some Transition Metal Carbides. *J. Phys. Chem.* **1958**, *62*, 630–631. [CrossRef]
30. Jun, C.K. Thermal Expansion of NbC, HfC, and TaC at High Temperatures. *J. Appl. Phys.* **2003**, *41*, 5081. [CrossRef]
31. Jun, C.K.; Shaffer, P.T.B. Thermal expansion of niobium carbide, hafnium carbide and tantalum carbide at high temperatures. *J. Less Common Met.* **1971**, *24*, 323–327. [CrossRef]
32. Lu, X.-G.; Selleby, M.; Sundman, B. Calculations of thermophysical properties of cubic carbides and nitrides using the Debye–Grüneisen model. *Acta Mater.* **2007**, *55*, 1215–1226. [CrossRef]
33. Yang, J.; Gao, F. First principles calculations of mechanical properties of cubic 5d transition metal monocarbides. *Phys. B Condens. Matter* **2012**, *407*, 3527–3534. [CrossRef]
34. Li, H.; Zhang, L.; Zeng, Q.; Guan, K.; Li, K.; Ren, H.; Liu, S.; Cheng, L. Structural, elastic and electronic properties of transition metal carbides TMC (TM=Ti, Zr, Hf and Ta) from first-principles calculations. *Solid State Commun.* **2011**, *151*, 602–606. [CrossRef]
35. Zeng, Q.; Peng, J.; Oganov, A.R.; Zhu, Q.; Xie, C.; Zhang, X.; Dong, D.; Zhang, L.; Cheng, L. Prediction of stable hafnium carbides: Stoichiometries, mechanical properties, and electronic structure. *Phys. Rev. B* **2013**, *88*, 214107. [CrossRef]
36. He, L.F.; Lin, Z.J.; Wang, J.Y.; Bao, Y.W.; Zhou, Y.C. Crystal structure and theoretical elastic property of two new ternary ceramics $Hf_3Al_4C_6$ and $Hf_2Al_4C_5$. *Scr. Mater.* **2008**, *58*, 679–682. [CrossRef]
37. Skundric, T.; Schön, J.C.; Zarubica, A.; Fonovic, M.; Zagorac, D. Exploring the energy landscape and crystal structures of $CrSi_2N_4$. *Z. Für Anorg. Und Allg. Chem.* **2023**, *649*, e202300130. [CrossRef]
38. Schön, J.C. Nanomaterials—What energy landscapes can tell us. *Process. Appl. Ceram.* **2015**, *9*, 157–168. [CrossRef]
39. Bergerhoff, G.; Brown, I.D. *Crystallographic Databases*; International Union of Crystallography: Chester, UK, 1987.
40. Zagorac, D.; Muller, H.; Ruehl, S.; Zagorac, J.; Rehme, S. Recent developments in the Inorganic Crystal Structure Database: Theoretical crystal structure data and related features. *J. Appl. Crystallogr.* **2019**, *52*, 918–925. [CrossRef]
41. Zagorac, D.; Doll, K.; Zagorac, J.; Jordanov, D.; Matović, B. Barium Sulfide under Pressure: Discovery of Metastable Polymorphs and Investigation of Electronic Properties on ab Initio Level. *Inorg. Chem.* **2017**, *56*, 10644–10654. [CrossRef]
42. Čančarević, Ž.P.; Schön, J.C.; Jansen, M. Stability of Alkali Metal Halide Polymorphs as a Function of Pressure. *Chem.—Asian J.* **2008**, *3*, 561–572. [CrossRef]
43. Dovesi, R.; Erba, A.; Orlando, R.; Zicovich-Wilson, C.M.; Civalleri, B.; Maschio, L.; Rérat, M.; Casassa, S.; Baima, J.; Salustro, S.; et al. Quantum-mechanical condensed matter simulations with CRYSTAL. *WIREs Comput. Mol. Sci.* **2018**, *8*, e1360. [CrossRef]
44. Dovesi, R.; Pascale, F.; Civalleri, B.; Doll, K.; Harrison, N.M.; Bush, I.; D'Arco, P.; Noël, Y.; Rérat, M.; Carbonnière, P.; et al. The CRYSTAL code, 1976–2020 and beyond, a long story. *J. Chem. Phys.* **2020**, *152*, 204111. [CrossRef] [PubMed]
45. Doll, K.; Saunders, V.R.; Harrison, N.M. Analytical Hartree–Fock gradients for periodic systems. *Int. J. Quantum Chem.* **2001**, *82*, 1–13. [CrossRef]
46. Doll, K.; Dovesi, R.; Orlando, R. Analytical Hartree-Fock gradients with respect to the cell parameter for systems periodic in three dimensions. *Theor. Chem. Acc.* **2004**, *112*, 394–402. [CrossRef]
47. Perdew, J.P.; Zunger, A. Self-interaction correction to density-functional approximations for many-electron systems. *Phys. Rev. B* **1981**, *23*, 5048–5079. [CrossRef]
48. Perdew, J.P.; Burke, K.; Ernzerhof, M. Generalized Gradient Approximation Made Simple. *Phys. Rev. Lett.* **1996**, *77*, 3865–3868. [CrossRef] [PubMed]
49. Monkhorst, H.J.; Pack, J.D. Special points for Brillouin-zone integrations. *Phys. Rev. B* **1976**, *13*, 5188–5192. [CrossRef]
50. Dovesi, R.; Saunders, V.; Roetti, C.; Orlando, R.; Zicovich-Wilson, C.; Pascale, F.; Civalleri, B.; Doll, K.; Harrison, N.; Bush, I. *CRYSTAL17 User's Manual*; University of Torino: Torino, Italy, 2017.
51. Doll, K. Gaussian Basis Sets for Solid State Calculations. In *Basis Sets in Computational Chemistry*; Perlt, E., Ed.; Springer International Publishing: Cham, Switzerland, 2021; pp. 157–181.
52. Ramo, D.M.; Gavartin, J.L.; Shluger, A.L.; Bersuker, G. Spectroscopic properties of oxygen vacancies in monoclinic $HfO_2$ calculated with periodic and embedded cluster density functional theory. *Phys. Rev. B* **2007**, *75*, 205336. [CrossRef]
53. Catti, M.; Pavese, A.; Dovesi, R.; Saunders, V.R. Static lattice and electron properties of $MgCO_3$ (magnesite) calculated by ab initio periodic Hartree-Fock methods. *Phys. Rev. B Condens. Matter* **1993**, *47*, 9189–9198. [CrossRef] [PubMed]
54. Skundric, T.; Matovic, B.; Zarubica, A.; Chudoba, D.; Zagorac, D. Data Mining Ab Initio Study of Gypsum $CaCO_3$ Modifications at Standard and Extreme Conditions. *J. Innov. Mater. Extrem. Cond.* **2023**, *4*, 38–51.
55. Hundt, R. *KPLOT, A Program for Plotting and Analyzing Crystal Structures*; Technicum Scientific Publishing: Stuttgart, Germany, 2016.
56. Momma, K.; Izumi, F. VESTA 3 for three-dimensional visualization of crystal, volumetric and morphology data. *J. Appl. Crystallogr.* **2011**, *44*, 1272–1276. [CrossRef]
57. Perger, W.F.; Criswell, J.; Civalleri, B.; Dovesi, R. Ab-initio calculation of elastic constants of crystalline systems with the CRYSTAL code. *Comput. Phys. Commun.* **2009**, *180*, 1753–1759. [CrossRef]
58. Erba, A.; Mahmoud, A.; Orlando, R.; Dovesi, R. Elastic properties of six silicate garnet end members from accurate ab initio simulations. *Phys. Chem. Miner.* **2014**, *41*, 151–160. [CrossRef]
59. Krikorian, N.H.; Wallace, T.C.; Anderson, J.L. Low-Temperature Thermal Expansion of the Group 4a Carbides. *J. Electrochem. Soc.* **1963**, *110*, 587. [CrossRef]

60. Aigner, K.; Lengauer, W.; Rafaja, D.; Ettmayer, P. Lattice parameters and thermal expansion of Ti($C_xN_{1-x}$), Zr($C_xN_{1-x}$), Hf($C_xN_{1-x}$) and $TiN_{1-x}$ from 298 to 1473 K as investigated by high-temperature X-ray diffraction. *J. Alloys Compd.* **1994**, *215*, 121–126. [CrossRef]
61. Lengauer, W.; Binder, S.; Aigner, K.; Ettmayer, P.; Guillou, A.; Debuigne, J.; Groboth, G. Solid state properties of group IVb carbonitrides. *J. Alloys Compd.* **1995**, *217*, 137–147. [CrossRef]
62. Zhang, H.; Hedman, D.; Feng, P.; Han, G.; Akhtar, F. A high-entropy $B_4$(HfMo$_2$TaTi)C and SiC ceramic composite. *Dalton Trans.* **2019**, *48*, 5161–5167. [CrossRef] [PubMed]
63. Feng, W.; Cui, S.; Hu, H.; Zhang, G.; Lv, Z. Electronic structure and elastic constants of $TiC_xN_{1-x}$, $Zr_xNb_{1-x}C$ and $HfC_xN_{1-x}$ alloys: A first-principles study. *Phys. B Condens. Matter* **2011**, *406*, 3631–3635. [CrossRef]
64. Razumovskiy, V.I.; Popov, M.N.; Ding, H.; Odqvist, J. Formation and interaction of point defects in group IVb transition metal carbides and nitrides. *Comput. Mater. Sci.* **2015**, *104*, 147–154. [CrossRef]
65. Yang, Y.; Ma, L.; Gan, G.-Y.; Wang, W.; Tang, B.-Y. Investigation of thermodynamic properties of high entropy (TaNbHfTiZr)C and (TaNbHfTiZr)N. *J. Alloys Compd.* **2019**, *788*, 1076–1083. [CrossRef]
66. Chang, Y.H.R.; Yoon, T.L. Effects of nitrogen addition and growth condition on the enhanced mechanical properties of transition metal carbides TMC (TM = Zr, Hf). *Ceram. Int.* **2020**, *46*, 1124–1136. [CrossRef]
67. Jiang, S.; Shao, L.; Fan, T.-W.; Duan, J.-M.; Chen, X.-T.; Tang, B.-Y. Elastic and thermodynamic properties of high entropy carbide (HfTaZrTi)C and (HfTaZrNb)C from ab initio investigation. *Ceram. Int.* **2020**, *46*, 15104–15112. [CrossRef]
68. Krasnenko, V.; Brik, M. First-principles calculations of the structural, elastic and electronic properties of $MN_xC_{1-x}$ (M=Ti, Zr, Hf; 0<x<1) carbonitrides at ambient and elevated hydrostatic pressure. *Solid State Sci.* **2013**, *28*, 1–8.
69. Kim, J.; Kwon, H.; Kim, B.; Suh, Y. Finite temperature thermal expansion and elastic properties of ($Hf_{1-x}Ta_x$)C ultrahigh temperature ceramics. *Ceram. Int.* **2019**, *45*, 10805–10809. [CrossRef]
70. Schön, J.C.; Jansen, M. Determination of candidate structures for simple ionic compounds through cell optimisation. *Comput. Mater. Sci.* **1995**, *4*, 43–58. [CrossRef]
71. Zagorac, D.; Zagorac, J.; Fonović, M.; Prikhna, T.; Matović, B. Novel boron-rich aluminum nitride advanced ceramic materials. *Int. J. Appl. Ceram. Technol.* **2023**, *20*, 174–189. [CrossRef]
72. Haq, B.U.; AlFaify, S.; Alrebdi, T.A.; Ahmed, R.; Al-Qaisi, S.; Taib, M.F.M.; Naz, G.; Zahra, S. Investigations of optoelectronic properties of novel ZnO monolayers: A first-principles study. *Mater. Sci. Eng. B* **2021**, *265*, 115043. [CrossRef]
73. Guinier, A.; Bokij, G.B.; Boll-Dornberger, K.; Cowley, J.M.; Durovic, S.; Jagodzinski, H.; Krishna, P.; de Wolff, P.M.; Zvyagin, B.B.; Cox, D.E.; et al. Nomenclature of polytype structures. Report of the International Union of Crystallography Ad hoc Committee on the Nomenclature of Disordered, Modulated and Polytype Structures. *Acta Crystallogr. Sect. A* **1984**, *40*, 399–404. [CrossRef]
74. Kelly, J.F.; Fisher, G.R.; Barnes, P. Correlation between layer thickness and periodicity of long polytypes in silicon carbide. *Mater. Res. Bull.* **2005**, *40*, 249–255. [CrossRef]
75. Aksenov, S.M.; Charkin, D.O.; Banaru, A.M.; Banaru, D.A.; Volkov, S.N.; Deineko, D.V.; Kuznetsov, A.N.; Rastsvetaeva, R.K.; Chukanov, N.V.; Shkurskii, B.B.; et al. Modularity, polytypism, topology, and complexity of crystal structures of inorganic compounds (Review). *J. Struct. Chem.* **2023**, *64*, 1797–2028.
76. Zagorac, D.; Schön, J.C.; Zagorac, J.; Jansen, M. Theoretical investigations of novel zinc oxide polytypes and in-depth study of their electronic properties. *RSC Adv.* **2015**, *5*, 25929–25935. [CrossRef]
77. Menad, A.; Benmalti, M.E.; Zaoui, A.; Ferhat, M. Impact of polytypism on the ground state properties of zinc oxide: A first-principles study. *Results Phys.* **2020**, *18*, 103316. [CrossRef]
78. Zagorac, D.; Doll, K.; Schön, J.C.; Jansen, M. Ab initio structure prediction for lead sulfide at standard and elevated pressures. *Phys. Rev. B* **2011**, *84*, 045206. [CrossRef]
79. Mudring, A.-V. Thallium Halides—New Aspects of the Stereochemical Activity of Electron Lone Pairs of Heavier Main-Group Elements. *Eur. J. Inorg. Chem.* **2007**, *2007*, 882–890. [CrossRef]
80. Lowndes, R.P.; Perry, C.H. Molecular structure and anharmonicity in thallium iodide. *J. Chem. Phys.* **1973**, *58*, 271–278. [CrossRef]
81. Yang, J.; Gao, F. Hardness calculations of 5d transition metal monocarbides with tungsten carbide structure. *Phys. Status Solidi B* **2010**, *247*, 2161–2167. [CrossRef]
82. Yu, R.; Wu, Q.; Fang, Z.; Weng, H. From Nodal Chain Semimetal to Weyl Semimetal in HfC. *Phys. Rev. Lett.* **2017**, *119*, 036401. [CrossRef]
83. Chung, D.H.; Buessem, W.R. The Voigt-Reuss-Hill Approximation and Elastic Moduli of Polycrystalline MgO, $CaF_2$, β-ZnS, ZnSe, and CdTe. *J. Appl. Phys.* **1967**, *38*, 2535–2540. [CrossRef]
84. Brown, H.L.; Armstrong, P.E.; Kempter, C.P. Elastic Properties of Some Polycrystalline Transition-Metal Monocarbides. *J. Chem. Phys.* **1966**, *45*, 547–549. [CrossRef]
85. Nartowski, A.M.; Parkin, I.P.; MacKenzie, M.; Craven, A.J.; MacLeod, I. Solid state metathesis routes to transition metal carbides. *J. Mater. Chem.* **1999**, *9*, 1275–1281. [CrossRef]
86. Isaev, E.I.; Simak, S.I.; Abrikosov, I.A.; Ahuja, R.; Vekilov, Y.K.; Katsnelson, M.I.; Lichtenstein, A.I.; Johansson, B. Phonon related properties of transition metals, their carbides, and nitrides: A first-principles study. *J. Appl. Phys.* **2007**, *101*, 123519. [CrossRef]
87. Zaoui, A.; Bouhafs, B.; Ruterana, P. First-principles calculations on the electronic structure of $TiC_xN_{1-x}$, $Zr_xNb_{1-x}C$ and $HfC_xN_{1-x}$ alloys. *Mater. Chem. Phys.* **2005**, *91*, 108–115. [CrossRef]

88. Krajewski, A.; D'Alessio, L.; De Maria, G. Physico-Chemical and Thermophysical Properties of Cubic Binary Carbides. *Cryst. Res. Technol.* **1998**, *33*, 341–374. [CrossRef]
89. Pierson, H.O. 4—Carbides of Group IV: Titanium, Zirconium, and Hafnium Carbides. In *Handbook of Refractory Carbides and Nitrides*; Pierson, H.O., Ed.; William Andrew Publishing: Westwood, NJ, USA, 1996; pp. 55–80.